Dynamic Characteristics Control of 2-DOF Manipulator with Artificial Muscles and Differential Gear using Disturbance Observer

T. Watanabe, D. Kamo, D. Tanaka, T. Nakamura and H. Osumi
Department of Precision Mechanics, Chuo University, 1-13-27 Kasuga, Bunkyo-ku, Tokyo 112-8551, Japan

Keywords: Artificial Muscle, Differential Gear, Disturbance Observer, Nominal Model.

Abstract: Recently, the demand for robots that operate in the fields of nursing and human life have increased due to the aging population and falling birthrates. Since these robots are intended to operate near humans, it is necessary they should have increased safety measures. Moreover, since it is desired that these robots use actuators that are light and soft, in several cases artificial muscles have been used as actuators. However, the Mckibben-type artificial muscles that are most commonly used have several drawbacks. Therefore, we developed a straight-fiber-type artificial muscle that was utilized to construct a two degree-of-freedom (2-DOF) manipulator. Because the manipulator is equipped with a differential gear mechanism, it is capable of performing 2-DOF bending and torsion motions using only one mechanism. However, the rotation speed of gears respectively differs in this mechanism, so the interference occurs in unintended directions because the speed of contraction and extension of the artificial muscle respectively differs. To address this problem, we introduce the disturbance observer (DOB) in the control system. Finally, we show that using our proposed DOB control method results in less interference in the 2-DOF manipulator than when using the proportional integral (PI) control method.

1 INTRODUCTION

In recent years, the number of older people requiring nursing has increased. However, the number of young people working in nursing homes has decreased. Therefore, the demand for robots that can provide medical treatment and assistance in nursing homes has increased. However, in order to decrease the effect of collisions, these robots should have safety and flexibility compared to currently used robots.

To satisfy these requirements, several robots use pneumatic artificial muscles as actuators. The most commonly used pneumatic artificial muscles are the Mckibben-type (Klute et al., 1999); (Tondu and Zagal, 2006); (Bong-Soo et al., 2009). However, Mckibben-type muscles have problems in regards to low durability and lack of output. Pleated pneumatic artificial muscles (Daerden et al., 2001) is that the radial expantion is large, and are not flexible we require, because they are not made from rubber. Therefore, in this study, we adopt the straight-fiber-type pneumatic artificial muscles that we developed in prior work (Nakamura et al., 2003). It has been experimentally and theoretically shown that these type of artificial muscles have a greater contraction ratio and more power than conventional McKibben-type muscles (Chou and Hannaford, 1994); (Nakamura, 2006). Moreover, because the straight-fiber-type muscles be made of rubber, they are extremely high durability, lightweight and flexible. They can be used to construct manipulators that have greater drivable range and torque. In addition, to compensate for the nonlinear properties of the artificial muscle, we applied a mechanical equilibrium model as a feedforward controller (Nakamura and Shinohara, 2007); (Nakamura and Maeda, 2008).

Using a straight-fiber-type pneumatic artificial muscle, we developed a six degrees of freedom (6-DOF) manipulator (Maeda et al., 2009). In order to achieve a more precice movement similar to humans, we want to extend the manipulator to have 7-DOF. In addition to an extra degree of freedom, we also want this manipulator to be flexible and light. Consequently, the mechanism of this manipulator needs to be compact. Thus, we developed a 2-DOF artificial muscle manipulator with a differential gear mechanism (Kamo et al., 2011). Consequently, the bending and rotation motion, as well as their

Watanabe T., Kamo D., Tanaka D., Nakamura T. and Osumi H..
Dynamic Characteristics Control of 2-DOF Manipulator with Artificial Muscles and Differential Gear using Disturbance Observer.
DOI: 10.5220/0004426801220129
In *Proceedings of the 10th International Conference on Informatics in Control, Automation and Robotics* (ICINCO-2013), pages 122-129
ISBN: 978-989-8565-71-6

stiffness can be controlled by a single mechanism. This differential gear mechanism drives by contracting antagonistic artificial muscles.

However, the speeds of contraction and expansion of the artificial muscles differ. Therefore, since the rotational speeds of the right and left gears in this mechanism are different, interference in unintended directions occurs, as shown in Figure 1.

To address this problem, we introduce in the control system the disturbance observer (DOB). The DOB provides robustness by estimating the disturbance and using feedback to cancel it (Wakui et al., 2012). For example, the DOB is used to control the joints of humanoid robots and enables them to walk stably even if the model mismatch and vibrations presense (Xing et al., 2010). Furthermore, the DOB has been used for backlash compensation of a DC motor (Jung et al., 2004). Moreover, the DOB can be used to force the output response to follow a nominal model. The angle response of the right (left) gear can be corresponded with that of left (right) gear, and consequently decrease interferences in unintended directions.

The remainder of this paper is organized as follows: In Section 2, we describe the shape of the muscle and its characteristics. In Section 3, we provide an introduction to DOB theory. In Section 4, we describe the mechanism of the 2-DOF artificial muscle manipulator with differential gears and its control system. In Section 5, we conduct experiments to compare the PI and DOB conrtollers and validate the effectivness of the DOB control method. Section 6 provides a summary and concluding remarks.

2 STRAIGHT-FIBER-TYPE PNEUMATIC ARTIFICIAL MUSCLE

2.1 Straight-fiber-type Pneumatic Artificial Muscle

Figure 2 shows a schematic of the straight-fiber-type artificial muscle. The tube shown is made of natural latex rubber and a carbon fiber sheet that is inserted along the direction of the long-axis. The two ends of the tube are fixed by terminals. Therefore, the artificial muscle expands in the radial direction and contracts in the axial direction when air pressure applies.

In Figures 3 and 4, we compare the pressure characteristics of the Mckibben-type and straight-fiber-type artificial muscles as a function of the contraction force and rate of contraction, respectively. We observe that the inner diameter and the length of both types of artificial muscles are the same size as shown in Figure 3. However, the straight-fiber-type artificial muscle produces a larger contraction force and rate of contraction than the McKibben-type artificial muscle. This difference occurs because the former muscle restricts expansion only in the axial direction, whereas the reticular fiber structure of the latter restricts expansion in both the axial and radial directions.

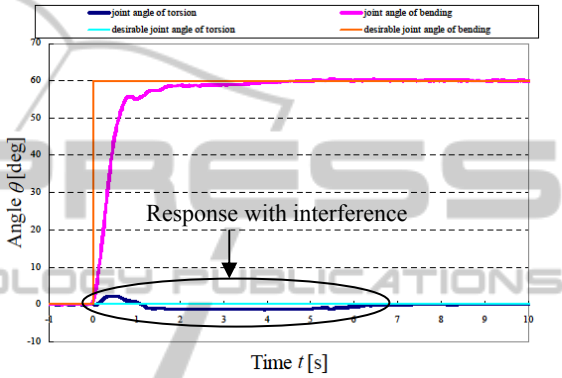

Figure 1: Experimental results from controlling the joint angle during a bending motion.

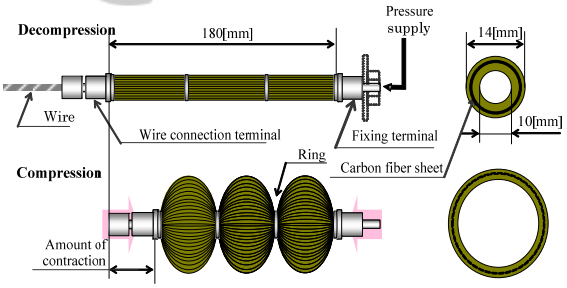

Figure 2: Straight-fiber-type pneumatic artificial muscle.

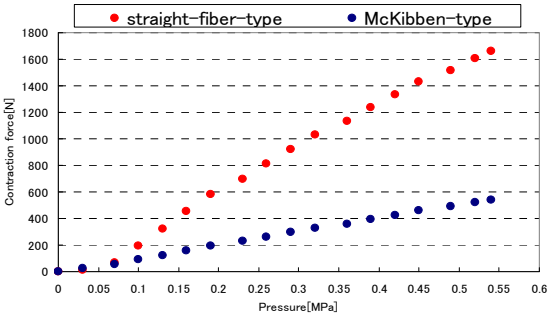

Figure 3: Relationship between pressure and contraction force.

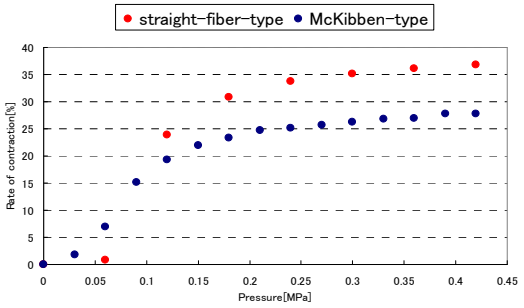

Figure 4: Relationship between pressure and rate of contraction.

2.2 Mechanical Equilibrium Model

The straight-fiber-type artificial muscle we developed has highly nonlinear characteristics. Moreover, because the gains of the input and output angles are unequal and the position control tends to be unstable. Therefore, we use the mechanical equilibrium model to linearize it (Nakamura, 2007; Nakamura and Maeda, 2008). The equations of the model are expressed as

$$P_1(\theta_d,\tau,K_{jd}) = [G_{11}(\varphi_{01})G_{22}(\varphi_{02}) - G_{12}(\varphi_{02})G_{12}(\varphi_{01}) \leq + \frac{K_{jd}}{K_{a2}}G_{21}(\varphi_{01})G_{32}(\varphi_{02}) + \frac{\tau}{r}G_{21}(\varphi_{01})G_{22}(\varphi_{02})] / \left[G_{22}(\varphi_{02})G_{31}(\varphi_{01}) + \frac{K_{a1}}{K_{a2}}G_{21}(\varphi_{01})G_{32}(\varphi_{02})\right] \quad (1)$$

$$P_2(\theta_d,\tau,K_{jd}) = \frac{K_{jd}}{K_{a2}} - \frac{K_{a1}}{K_{a2}}P_1 \quad (2)$$

$$\phi_{0i}(x_{di}') = \frac{2\alpha_i l_{0i}^{1.5} x_{di}'^{0.5}}{(l_{0i} - x_{di}')^2 + \alpha_i^2 x_{di}' l_{0i}} \quad (3)$$

$$G_{1i}(\phi_{0i}) = \frac{4K_{ai}t_i}{d_{0i}}\left[\frac{l_{0i}}{d_{0i}}\right]^2\left[\frac{\sin\phi_{0i} - \phi_{0i}\cos\phi_{0i}}{\phi_{0i}^2}\right] \quad (4)$$

$$G_{2i}(\phi_{0i}) = \frac{M\tan\phi_{0i}}{d_{0i}nb_i} \quad (5)$$

$$G_{3i}(\phi_{0i}) = 2\left[\frac{l_{0i}}{d_{0i}}\right]\left[\frac{\phi_0 - \sin\phi_{0i}\cos\phi_{0i}}{\phi_{0i}^2}\right] + 4\frac{l_{0i}}{d_{0i}}\frac{\sin\phi_{0i}}{\phi_{0i}} - \frac{M\pi d_{0i}}{nb_i}\tan\phi_{0i} \quad (6)$$

$$x_{d1}' = \frac{r\psi_1 - r\theta_d}{3} \quad (7)$$

$$x_{d2}' = \frac{r\psi_2 + r\theta_d}{3} \quad (8)$$

In Table 1, we present the parameters of these equations. The subscript number is used to discriminate between artificial muscles 1 and 2. When the same equation is used for both muscles, we use subscript i. Here, θ and θ_d represent the pulley angle and desirable value, respectively. P_1 and P_2, computed from Equations (1) and (2), respectively, are the pressure values required to realize θ_d. Therefore, θ and θ_d have a linear relationship. And then, torque is fed back to those equations. In this study, we use equilibrium model linearization (EML) to perform compensation. Therefore, we can express EML in the control system as a linear transfer function.

Moreover, we can control the joint stiffness K_j by inputting a desirable value K_{jd}. If the stiffness characteristic constants K_{a1} and K_{a2} are equal, the joint stiffness K_j is proportional to the initial pressure P_0. Thus, we can select the joint stiffness we desire.

Figure 5 shows a comparison between theoretical and experimental results of the relationship between force applied and contraction observed. This result shows that the experimental results are in agreement with the theory. Hence, the mechanical equilibrium model provides the sufficient accuracy required to perform position and stiffness control.

Table 1: Parameter of EML.

θ_d	[rad]	Desirable angle
τ	[Nm]	Load torque
P_1 / P_2	[Pa]	Pressure
ϕ_{01} / ϕ_{02}	[rad]	The central angle of the arc shape of the muscle
x_{d1} / x_{d2}	[m]	Desirable contraction
ψ_1 / ψ_2	[rad]	Angle of slack wire
b_i	[mm]	Width of glass fiber
α_i		Approximation constant number

r	[mm]	Radius of the pulley
n		Number of the glass fiber
K_j	[Nm/rad]	Joint Stiffness
K_{a1} / K_{a2}		Fixed stiffness number
l_{0i}	[m]	Length between cap and ring
d_{0i}	[m]	Diameter of artificial muscle
t_i	[m]	Thickness of artificial muscle
M		Fiber constant number

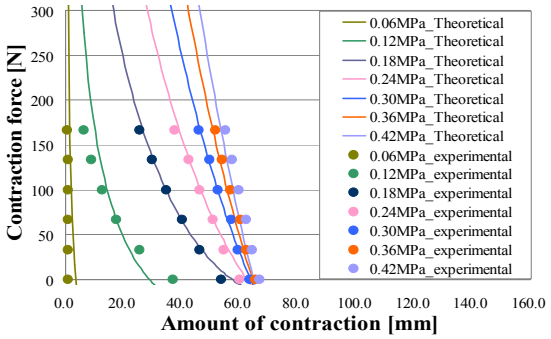

Figure 5: Comparison between theoretical and experimental results of the relationship between force applied and contraction observed.

3 DISTURBANCE OBSERVER THEORY

To date, we have used a PI controller to control the position of the 2-DOF manipulator. However, because the PI controller cannot compensate for the dynamic characteristics of the system, we apply the DOB here.

3.1 Disturbance Observer Theory

Figure 6 shows a block diagram of the DOB (Wakui et al., 2012). The DOB is composed of the plant, the inverse of the plant, and a filter. The nominal model represents the transfer function of the ideal response, which is arbitrarily selected. The DOB operates as follows. First, it uses the difference between the ideal input and actual response to estimate the disturbance. Second, the estimated disturbance passes through the filter and is used as feedback. Therefore, because the disturbance is canceled, the output becomes equal to the input. If the transfer function of the filter is $F(s) = 1$, the relation between the input and output is expressed by Equation (9).

$$y(s) = P_n(s)r(s) \tag{9}$$

While a mismatch between the output of the plant and the desirable value (output of the nominal model) is detected, feedback is performed and the output value changes according to Equation (9).

Therefore, we can control the interference in unintended directions because the angle response of the right and left gears corresponds with the nominal model.

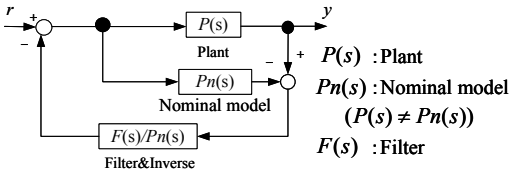

Figure 6: Block diagram of DOB.

3.2 Filter Design Theory

The transfer function of filter $F(s)$ is expressed by Equation (10).

$$F(s) = \frac{1}{(Ts+1)^n} \tag{10}$$

Here, T is an arbitrary parameter representing the time constant of the filter. For the system to be stable, the degree of the filter n must be greater than or equal to that the degree of $P_n(s)$.

4 2-DOF MANIPULATOR WITH DIFFERENTIAL GEAR MECHANISM

4.1 2-DOF Manipulator with Differential Gear Mechanism

In Figure 7, we present the 2-DOF manipulator with a differential gear mechanism used in this study. The upper arm, the lower arm and the weight of the manipulator are 310 mm, 260 mm and around 2.5 kg respectively. And then, the manipulator is mainly composed of two pairs of antagonistic artificial muscles and a differential gear. The antagonistic artificial muscles are connected by a wire through a pulley.

In Figure 7 (b) and (c), we illustrate the motions the manipulator can perform. When bevel gears A and B rotate in opposite directions, bevel gear C is fixed around the x-axis and rotates around the z-axis. In this study, this motion of the manipulator is termed as torsion motion. When bevel gears A and B rotate in the same direction, bevel gear C is fixed around the z-axis and rotates around the x-axis with bevel gears A and B. In this study, this motion of the manipulator is termed as bending motion.

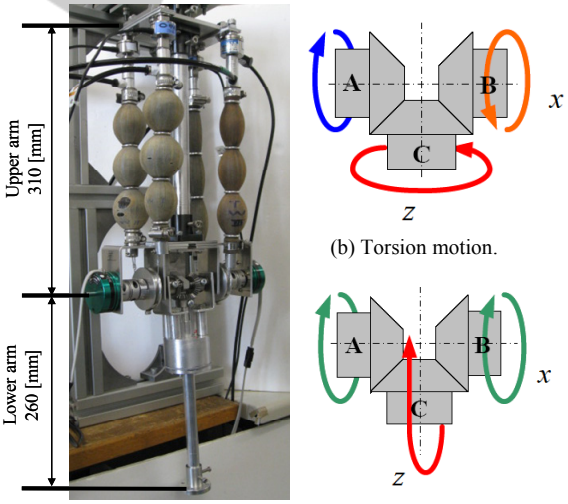

(a) 2-DOF manipulator. (b) Torsion motion. (c) Bending motion.

Figure 7: 2-DOF manipulator with differential gear mechanism.

4.2 Experimental System

Figure 8 shows a schematic of the experimental system used for the 2-DOF artificial muscle manipulator. The artificial muscles are connected to an air compressor via proportional solenoid valves.

Thus, we use the proportional solenoid valves to control the air pressure provided by the air compressor. The air pressure applied to each artificial muscle is controlled by a PC that is connected to the proportional solenoid valves. At equilibrium, a pressure of P_0 is applied to both muscles. When we apply a pressure of $+\Delta P$ to one artificial muscle and at the same time a pressure of $-\Delta P$ to the other, the pulleys begin to rotate because the contractile forces of the two artificial muscles differ. Moreover, the rotation of the pulley causes the differential gear to begin rotating, which in turn drives the 2-DOF artificial muscle manipulator.

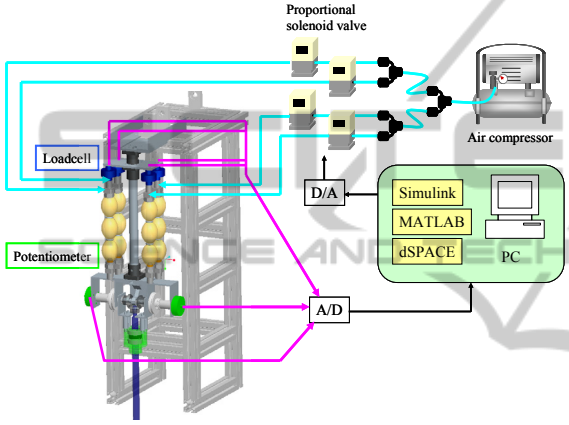

Figure 8: Schematic of the experimental system.

4.3 Control System

We designed a control system for the manipulator using Simulink. The control inputs were applied using dSPACE. Figure 9 shows the block diagram of the manipulator control system. We introduced the DOB in the control system to control the output angles of pulleys A and B. The controller considers all responses as disturbances, except those of the nominal model. We use the desirable bending angle θ_{dA}, desired torsion angle θ_{dB}, output angles θ_A and θ_B detected by the potentiometer, desirable joint stiffness k_{jd}, and load torque τ in the EML to compute the air pressure that should be applied to each artificial muscle.

We execute the torque feedback by using the load cell connected each artificial muscles. Because the force acting on each artificial muscle was measured by the load cell, we can calculate the load torque in one antagonistic artificial muscle by taking the force gap.

We showed the nominal model by dead time and the first-order system. We selected the nominal model by performing experiments using the PI controller and examining the response of the manipulator. From the experimental results, we concluded that the dead time was 0.02 s, and the time constant of the first-order system was 0.35. Next we analyzed the vibration and trajectory tracking performance of the system and set the time constant of filter to T = 0.5. Because the nominal model is expressed by a first-order system, we set the order of the filter to n = 1. In addition, because we want to compare the PI control with the DOB control, we set the desirable joint stiffness to a fixed value, k_{jd} = 0.08. The transfer functions of the nominal model P_n(s) and filter F(s), are expressed by Equations (11) and (12), respectively. The transfer function of the dead time is expressed using the Pade approximation.

$$P_n(s) = \frac{s^2 - 300s + 30000}{s^2 + 300s + 30000} \cdot \frac{1}{0.35s + 1} \quad (11)$$

$$F(s) = \frac{1}{0.5s + 1} \quad (12)$$

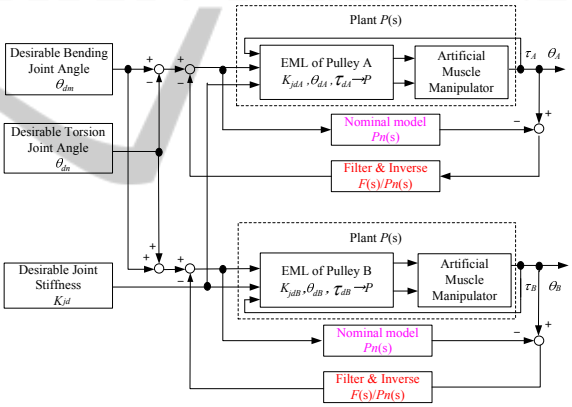

Figure 9: Block diagram of the manipulator control system.

5 JOINT ANGLE CONTROL EXPERIMENT AND EXAMINATION

First, we applied a 50 deg step signal as input for bending and torsion, while the manipulator had no load. Then, we repeated the same experiment with a manipulator load of 0.5 N.

5.1 Examination of Joint Angle Control Experiment

Here, we present the experimental results obtained and discuss our findings. We omit responses

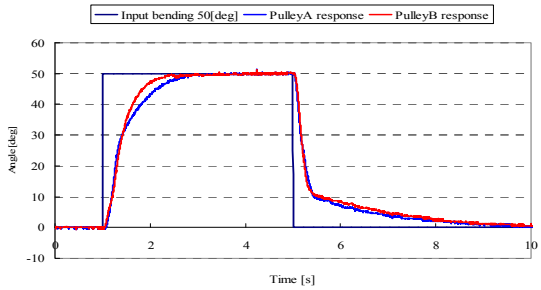

a) Responses of pulleys.

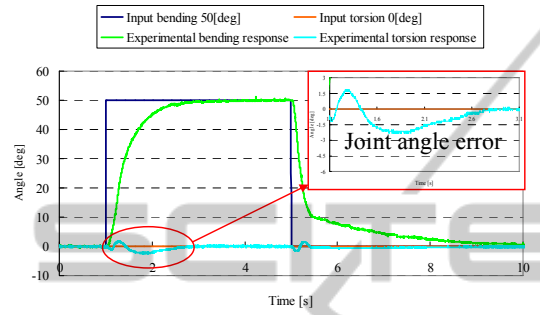

(b) Responses of joint angles.

Figure 10: Experimental results of bending motion while applying PI control.

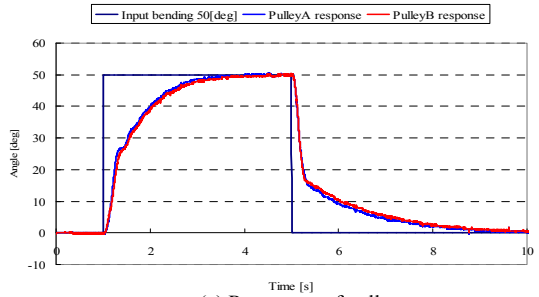

(a) Responses of pulleys.

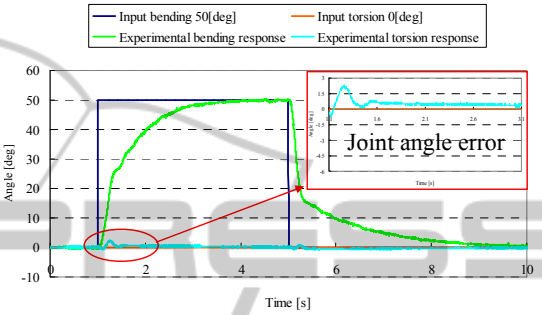

(b) Responses of joint angles.

Figure 11: Experimental results of bending motion while applying DOB control.

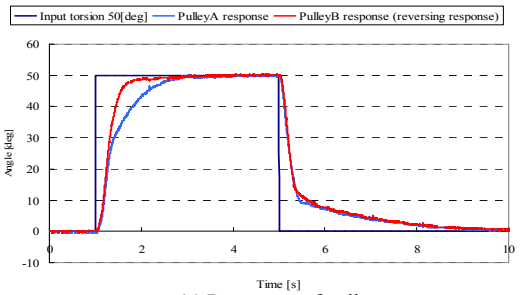

(a) Responses of pulleys.

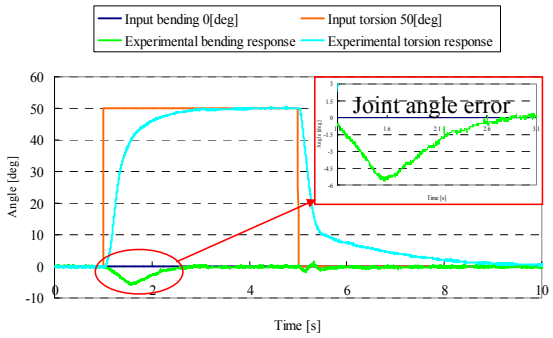

(b) Responses of joint angles.

Figure 12: Experimental results of torsion motion while applying PI control.

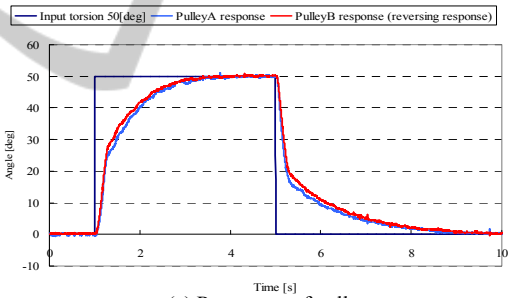

(a) Responses of pulleys.

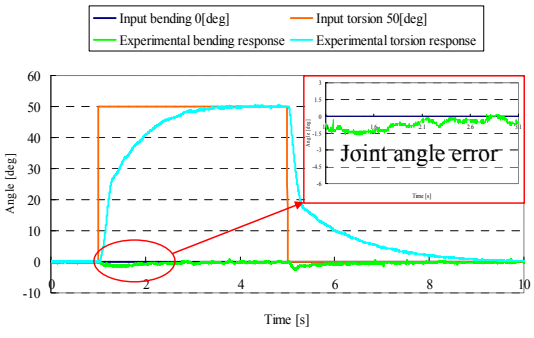

(b) Responses of joint angles.

Figure 13: Experimental results of torsion motion while applying DOB control.

obtained for a load of 0.5 N, because they are approximately equal to the ones obtained for no load.

In Figures 10-13, we present experimental results obtained when a 50 deg step signal was applied as

input for bending and torsion, while the manipulator had no load. Figure 10 shows experimental results for an input signal of bending of 50 deg, while applying PI control. Figure 10 (a) shows the angular responses of pulleys A and B, and Figure 10 (b) shows the response of the joint angle.

Next, we discuss differences between the PI and DOB control methods. In Figure 10 (b), we observe that the joint angle error occurs in the direction of torsion. This result is caused by the errors in the angular responses of pulleys A and B, as shown in Figure 10 (a).

In Figure 11, we present experimental results for an input signal of bending of 50 deg, while applying DOB control. In Figure 11 (b), we observe that the joint angle error in the direction of torsion has been reduced. This result occurs because the angular response of pulley A is approximately equal to that of pulley B, as shown in Figure 11 (a). Figures 12 and 13 present experimental results for an input signal of torsion of 50 deg, while applying PI and DOB control, respectively. The response of pulley B present by reversing the real response of it to compare the response, though the real response of pulley B is opposite to that of pulley A in torsion motion. Similar to the experimental results of bending motion, we observe that the joint angle error caused by torsion motion was also reduced with DOB control.

5.2 Examination and Comparison using the Area of the Joint Angle Error

Next, we evaluate the interference in unintended directions as the area of the joint angle error in the cases of no load and a load of 0.5 N.

In Figure 14, we present the evaluation results obtained for the area of the joint angle error. The area expresses by integrating the joint angle error per unit of time. The vertical axis shows amount of the joint angle error and the unit is assumed to be dimensionless. In Figure 14, it shows by hyphen.

First, we discuss differences between the PI and DOB control methods. From Figure 14, we observe that the area of the joint angle error when applying DOB control is smaller than when applying PI control. Specifically, the area of the error was reduced by approximately 40% in the case of an input signal of torsion of 50 deg and a load of 0.5 N. This result occurs because the angular response of pulley A is approximately equal to that of pulley B. Therefore, we conclude that DOB control successfully compensates for interferences in unintended directions.

Second, we discuss differences between the areas of error caused during bending and torsion motions. In our results, we observe that regardless of the load and control method used, the area of error of torsion is larger than that of bending. We explain this result by Figure 15. Figure 15 present the force caused in bevel gear C. Because the interference occurs in bending direction when applying torsion motion in Figure 12 and 13, the component of the gravity direction is assumed to act, as shown Figure 15 (b). And then, F_A and F_B represent the rotational force of bevel gears A and B, respectively. The interference in unintended direction occurs because the balance of the force in interference direction caused bevel gear C collapses. That is, the interference occurs because the force generated on bevel gears A side and B side differs respectively. In Figure 15, in bending motion, the gravity load f_g acts in the same direction for F_A and F_B, respectively. At this time, the interference is not easily generated because the resultant force on bevel gears A side and B side is the same, respectively. However, f_g acts in opposite direction for F_A, whereas f_g acts in the same direction for F_B in torsion motion. Therefore, because the resultant force on bevel gears A side and B side differs, respectively, the interference in torsion motion is easily generated than in bending motion. Thus, we conclude that this is the reason why the area of error in torsion is larger than that in bending.

Third, we examine the area of error of bending in the cases of no load and for a load of 0.5 N. From the results obtained, we see that the area of error of bending for a load of 0.5 N is smaller than that with no load. We believe that the manipulator could not rotate easily because the load restricted the motion of the torsion. For the same reason, the area of error of torsion in the case of a load of 0.5 N was smaller than that in the case for no load.

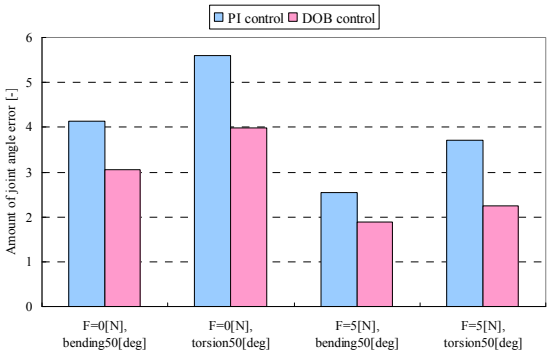

Figure 14: Area of error in the direction of interference.

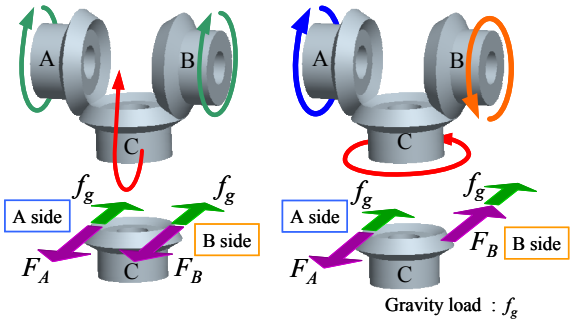

(a) Bending motion. (b) Torsion motion.

Figure 15: The force caused in bevel gear C.

On the basis of these results, we conclude that regardless of the presence of load, the DOB control is more effective than PI control in reducing the interference in unintended directions.

6 CONCLUSIONS

We adopted the DOB in the control system of a 2-DOF manipulator with straight-fiber-type artificial muscles and a differential gear mechanism. Experimental results show that regardless of the presence of load, the DOB control method performs better that the PI control in reducing the interference in unintended directions. Hence, we prove the effectiveness of our proposed DOB control method.

In the future, we apply the DOB control to a manipulator with multiple degrees of freedom and show that the interference is reduced even if the weight of the manipulator gains by increasing the degree of freedom.

REFERENCES

Bong-Soo, K., Kothera, C. S., Woods, B. K. S., Wereley, N. M. (2009). Dynamic modeling of Mckibben pneumatic artificial muscles for antagonistic actuation. in *Proceedings of IEEE International Conference on Robotics and Automation*, 12-17 May., pp.182-187.

Chou C. P. and Hannaford, B. (1994). Static and Dynamic Characteristics of McKibben Pneumatic Artificial Muscles. in *Proceedings of IEEE International Conference on Robotics and Automation*, San Diego, California, USA, 8-13 May, pp. 281-286.

Daerden, F., Lefeber, D., Verrelst, B. and Van Ham, R. (2001). Pleated Pneumatic Artificial Muscles: Compliant Robotic Actuators. in *Proceedings of IEEE/RSJ International Conference on Intelligent Robots and Systems,* Hawaii, USA, pp.1958-1963.

Jung, B. -J., Kong, J.–S., Lee, B.–H., Ahn, S.–M., Kim, J.–G. (2004). Backlash compensation for a humanoid robot using disturbance observer. in *Proceedings of 30th Annual Conference of IEEE on Industrial Electronics Society*, Busan, South Korea, 2-6 Nov., vol.3, pp. 2142- 2147.

Kamo, D., Maehara, M., Tanaka, D. and Nakamura, T. (2011). Development of a manipulator with straight-fiber-type artificial muscle and differential gear mechanism. *in Proceedings of 37th Annual Conference of IEEE on Industrial Electronics Society*, Melbourne, Australia, 7-10 Nov., pp.98-103.

Klute, G. K., Czernieki, J. M. and Hannaford, B. (1999). McKibben Artificial Muscles: Pneumatic Actuators with Biomechanical Intelligence. in *Proceedings of the IEEE/ASME International Conference on Advanced Intelligent Mechatronics*, Atlanta, USA, pp. 221-226.

Nakamura, T. (2006). Experimental Comparisons between McKibben type Artificial Muscles and Straight Fibers Type Artificial Muscles. *SPIE International Conference on Smart Structures, Devices and Systems III*, San Diego, California, USA

Nakamura, T. and Maeda, H. (2008). Position and Compliance Control of an Artificial Muscle Manipulator using a Mechanical Equilibrium Model. *in Proceedings of IEEE International Conference on Robotics and Automation*, Pasadena, California, USA, 10-13 Nov., pp. 3431-3436.

Nakamura, T., Saga, N. and Yaegashi, K. (2003). Development of Pneumatic Artificial Muscle based on Biomechanical Characteristics. *in Proceedings of IEEE International Conference on Industrial Technology*, Maribor, Slovenia, pp. 729-734.

Nakamura, T. and Shinohara, H. (2007). Position and Force Control Based on Mathematical Models of Pneumatic Artificial Muscles Reinforced by Straight Glass Fibers. *in Proceedings of IEEE International Conference on Robotics and Automation*, Roma, Italy, 10-14 April, pp. 4361-4366.

Maeda, H., Nagai, H., Nakamura, T. (2009). Development of a 6-DOF manipulator actuated with a straight-fiber-type artificial muscle. *in Proceedings of IEEE/RSJ International Conference on Intelligent Robots*, St. Louis, USA, 10-15 Oct., pp.607-612.

Tondu, B., Zagal, S. D. (2006). McKibben artificial muscle can be in accordance with the Hill skeletal muscle model. in *Proceedings of IEEE/RAS-EMBS International Conference on Biomedical Robotics and Biomechatronics*, 20-22 Feb., pp.714-720.

Wakui, S., Hashimoto, S., Takanashi, H., Nakamura, K. (2012). *Fundamentals of Control Engineering Available to Industry*, CORONA. Tokyo Japan, 1st edition.

Xing, D., Su, J., Liu, Y. and Zhong, J. (2011). Robust approach for humanoid joint control based on a disturbance observer. *Journal of Control Theory & Applications, IET*, 22 Sep., vol.5, no.14, pp.1630-1636.